ELSEVIER

Journal of Chromatography A, 944 (2002) 3–22

JOURNAL OF CHROMATOGRAPHY A

www.elsevier.com/locate/chroma

Effect of the homogeneity of the column set on the performance of a simulated moving bed unit
II. Experimental study

Kathleen Mihlbachler[a,b,c], Andreas Jupke[d], Andreas Seidel-Morgenstern[c], Henner Schmidt-Traub[d], Georges Guiochon[a,b,*]

[a]*Department of Chemistry, University of Tennessee, Knoxville, TN, USA*
[b]*Division of Chemical and Analytical Sciences, Oak Ridge National Laboratory, Oak Ridge, TN, USA*
[c]*Department of Chemical Engineering, O.-v.-Guericke University of Magdeburg, Magdeburg, Germany*
[d]*Department of Chemical Engineering, University of Dortmund, Dortmund, Germany*

Abstract

Previous studies of the simulated moving bed (SMB) process assume identical characteristics of all the columns incorporated in a given unit. Due to the practical impossibility to manufacture *identical* columns, numerical applications of the theory to modeling and optimization use for each of the needed column parameter the average value for the entire column set. In this study, the effects of these simplifications on the actual productivity of the SMB process are evaluated by making exact calculations, i.e., by taking the differences in the porosity values into account. We apply a revised set of separation conditions previously introduced and derived from the equilibrium theory. Earlier theoretical results are compared to experimental results obtained in the study of the enantiomeric separation of Tröger's base on Chiralpak AD. Due to the nonLangmuirian character of the adsorption isotherms of these two compounds on the packing material used, the separation area cannot be determined analytically. As an alternative, a reliable numerical algorithm was used to scan a wider region and to define the separation area. The form of this area depends on the applied porosity values. A UV detector and a laser polarimeter located at one node of the SMB monitor on-line the internal concentration profiles. Excellent agreement between the calculated and the experimentally determined concentration profiles was obtained under nonlinear conditions. The influence of column-to-column variations on the performance of the SMB process was found to be more significant under nonlinear than under linear conditions.

Keywords: Simulated moving bed chromatography; Porosity; Enantiomer separation; Adsorption isotherms; Mathematical modeling; Tröger's base

1. Introduction

The simulated moving bed (SMB) process has gained considerable interest in the separation of racemic mixtures over the last decade [1–5], especially after the statement made in the mid 1990s by the US Food and Drug Administration (FDA) concerning the purity of chiral compounds to be used as pharmaceuticals [6]. Although enantioselective synthesis is a valid alternative, the racemic mixture (50:50 of both enantiomers) is often much easier,

*Corresponding author. Department of Chemistry, University of Tennessee, 552 Buehler Hall, Knoxville, TN 37996-1600, USA. Tel.: +1-865-9740-733; fax: +1-865-9742-667.
E-mail address: guiochon@utk.edu (G. Guiochon).

0021-9673/02/$ – see front matter
PII: S0021-9673(01)01396-6

cheaper, and less time consuming to synthesize [7]. With help of an especially designed chiral stationary phase (CSP), this mixture can then be separated by a suitable high-performance liquid chromatography (HPLC) based process. Besides the SMB technology, preparative elution chromatography and close-looped recycle chromatography can be applied. Compared to elution chromatography, which is a batch process, continuous processes afford lower solvent consumption and higher productivity. The main disadvantage of the SMB process, its inability simply to separate mixtures into more than two fractions, disappears in the case of enantiomeric separations. Enantiomeric separations are characterized by much smaller specific capacities of the adsorbents, markedly lower values of the separation factors, and the absolute need to work under non-linear conditions in order to achieve an economically viable process.

Based on true moving bed chromatography (TMB), the SMB technology was patented by Broughton and Gerhold [8]. It overcomes the major practical disadvantages of moving the solid phase through the column, the impossibility of achieving a reasonable column efficiency and the progressive erosion of the solid-phase particles into dust. Column switching simulates the movement of the solid phase. Therefore, the SMB process shown in Fig. 1 is periodical. As a consequence, its performance varies from that of the true counter-current process [9].

All fundamental discussions regarding the modeling of SMB, its properties, and the optimization of its design and its operating conditions [9–15], have assumed that all the columns have identical characteristics. Although the same batch of packing material may be used to pack the columns, it is impossible to manufacture four, let alone more (e.g., eight, 12, or 16) identical columns [16]. Therefore, in the modeling of actual units and in calculations made to optimize them, the average values of the parameters for the entire column set are applied.

Column-to-column variations in the packing density cause changes in the retention times of compounds at constant flow-rate, hence in the positions of their band fronts at switching time. Variations in the packing density cause variations in the column porosity, as determined by the retention time of a nonadsorbed compound, and result into changes in

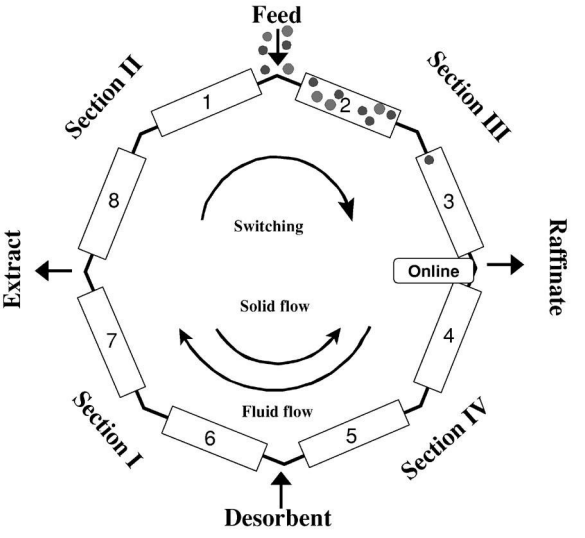

Fig. 1. Schematics of the SMB process including the online monitoring system.

the local mobile phase velocity. Because the process of packing particles in a column is not well understood, local fluctuations of the density are unavoidable and the distribution of these differences is not reproducible. Accordingly, column-to-column variations of the porosity and permeability are observed. Even columns packed by axial compression and filled with the same amount of the same packing material have slightly different retention times. The degree of reproducibility that can be achieved for the characteristics of small-size columns was previously discussed [16], Some of the effects of slight differences between the different columns of a set were also reported previously [17,18]. The most notable one was the observation of a superperiod for the composition of the column effluents, notably those of the raffinate and extract streams. This superperiod is the product of the basic SMB period and the total number of columns in the unit.

Mihlbachler et al. [19] made a theoretical evaluation of the influence of the lack of homogeneity of the column packing on the performance of the SMB process. As far as the operation of an SMB separator is concerned, the most important fluctuations are those of the retention factors (more than those of the column efficiency). The goal of this work was to check the validity of our initial, theoretical findings

by comparing them to the results of series of experimental runs. The model system is the separation under nonlinear conditions of the enantiomers of Tröger's base on a silica-based CSP coated with an amylose derivative, using isopropanol as the mobile phase. A most similar separation, that of the same enantiomers on cellulose microcrystalline triacetate, was studied by Seidel-Morgenstern and Guiochon [20]. These authors found that the equilibrium isotherm of the first enantiomer was Langmuirian, that of the second antiLangmuirian. They used the ideal adsorbed solution theory to account for the competitive adsorption. However, a systematic discrepancy was observed between the calculated and the measured band profiles of the racemic mixture under overloaded conditions [20].

The operating conditions of the SMB were determined with our revised set of separation conditions. Due to the adsorption behavior of this mixture on the packing material (see Sections 2.2, 2.3, 4.2, and 4.3.1), the separation area could not be determined analytically. As an alternative, a reliable numerical algorithm was used to scan a wider region and to define the separation area. The form of this area is related to the applied porosity values. The internal concentration profiles of the two components in our SMB process were both determined. This was achieved by combining the responses of two online detectors, a UV spectrophotometric detector and a laser polarimeter (see Fig. 1). Thus, a direct comparison of the experimental concentration profiles and of those calculated with either the exact porosity values or the set average was possible.

The combination of these two detectors has already been used in analytical chromatography, e.g., Refs. [21–24], and in preparative elution chromatography [25]. Recently, the use of this combination was described for the determination of the purities of the outlet streams of the SMB process [18]. So far, however, only the combination of the UV detector and a Raman spectroscopic detector has been used to monitor the internal concentration profiles of a racemic mixture within the SMB process [26]. However, there has been in recent meetings a growing interest in using this detector combination to validate the process parameters and to find the optimum operating conditions of SMB separations and some results will be published soon [27,28].

Finally, it is worth noting that other parameters, e.g., the column efficiency and the dead volumes [29], may also have a significant influence on the unit performance. However, we concentrate here on the porosity and assume that all the other parameters are kept constant.

2. Theory

The mathematical modeling of the SMB process is based on the first part of this work [19], which described the theoretical background of the SMB process and the adjustments required to take into account the exact properties of each column. More detailed information about the parameter phase ratio $F = (1 - \epsilon_t)/\epsilon_t$ can be found there and elsewhere [30,31]. This important model parameter is a function of the total column porosity.

In the following section, the mathematical modeling of the SMB process is summarized as used for the model system. The mass balance equations based on those of the equilibrium theory with their initial and boundary conditions and the phase equilibrium of the two components between the liquid and the solid phases describes the concentration distribution during the SMB process. The node equations are integral mass balance equations, which must be fulfilled at the nodes between the different sections of the SMB. Finally, the revised set of separation conditions is applied to reach complete separation of the feed mixture.

2.1. Equilibrium–dispersive model

The equilibrium–dispersive model describes the differential mass balance of component i ($i = 1, 2$) in section j ($j = \mathrm{I}, \mathrm{II}, \mathrm{III}, \mathrm{IV}$) and column k ($k = 1 \ldots, n$, with n total number of columns) in the SMB unit (see Fig. 1). This model assumes instantaneous equilibrium between the solid and liquid phases but accounts for the effects of a finite column efficiency, N. In contrast to the ideal model in which there is no axial dispersion, axial diffusion and the mass transfer resistances are included in the equilibrium–dispersive model. Mass transfers are assumed to be fast and to combine with those of axial diffusion into an apparent axial dispersion coefficient, D_{ap}. To sim-

plify the numerical calculations, we assume that the dispersion coefficient is the same for all components and is constant in all the columns of the SMB unit:

$$\frac{\partial C_{i,j,k}}{\partial t} + u_{j,k} \cdot \frac{\partial C_{i,j,k}}{\partial z} - D_{\mathrm{ap}} \cdot \frac{\partial^2 C_{i,j,k}}{\partial z^2} + F_k \cdot \frac{\partial q_{i,j,k}}{\partial t} = 0 \tag{1}$$

Knowing the column efficiency, the apparent dispersion coefficient can be derived from the following equation:

$$D_{\mathrm{ap}} = \frac{u_{j,k} L_{\mathrm{c}}}{2N_{j,k}} \tag{2}$$

where the mobile phase linear velocity, $u_{j,k}$, depends on the porosity of the corresponding column and on the section of the SMB in which this column is located. To ensure numerical stability in the calculation of the numerical solution of Eq. (1), the spatial increments used for the integration of the equation in each column *j*, *k* have to be adjusted depending on the linear velocity, $u_{j,k}$ and the minimum efficiency, $N_{\min}$. To solve the mass balance equations, the correct initial and boundary conditions must be defined (see Mihlbachler et al. [19]). The concentrations of the two components at the inlet of a section are defined by the mass balance equations of the corresponding node. In the literature, these mass balance equations are described and discussed extensively [9,12–14,17,32]. This node model combines the mass balance equation with the flow equation at each feed and draw-off node to realize simulated countercurrent in a series of columns. Note that the node model does not take into account the back mixing and the dispersion that take place between columns, in the connecting tubes, valves, and pumps of the SMB separator. In practice, these parts contribute significantly to band dispersion. These contributions must be included in any theoretical modeling, particularly those of units having large dead volumes [29].

After a certain time (equal to the SMB period), the feed and draw-off nodes are shifted to the next position in the fluid direction. This creates the simulated countercurrent motion of the solid phase. To account for this periodic changing of the feed and draw-off nodes, the boundary conditions of each column are updated accordingly at the beginning of each new cycle.

2.2. Isotherm equation

The solid-phase concentration, $q_{i,j,k}$ in Eq. (1), is related to the mobile phase concentration by the adsorption isotherm:

$$q_{i,j,k} = f(C_{1,j,k}, C_{2,j,k}) \tag{3}$$

where component 1 is assumed to be less retained than component 2 in the column, i.e., $a_1 < a_2$ and $\alpha = a_2/a_1 > 1$.

In many cases of nonlinear adsorption behavior [30], the relationship between solid and liquid phase concentrations can be described with the competitive Langmuir adsorption isotherm or with the related biLangmuir isotherm model. These isotherms account for the competitive interactions of the feed components with the solid phase. If a common saturation capacity, q_s, is assumed, the Langmuir isotherm model is thermodynamically consistent. Its equation is:

$$q_{i,j,k} = \frac{q_s b_i C_{i,j,k}}{1 + \sum_{l=1}^{M} b_l C_{l,j,k}} \tag{4}$$

Statistical thermodynamics [33,34] shows that the Langmuir isotherm is the first term of a series of possible isotherms of the form $q_i = q_s C_i P' \cdot (C_1, C_2)/P \cdot (C_1, C_2)$, where P is a polynomial of degree n and P' is its first derivative with respect to C_i. The second term of this series is the quadratic isotherm [30,35] which may be used to model adsorption isotherms that have an inflection point [36]. The following equations describe this isotherm model for a binary mixture:

$$q_1 = \frac{q_s C_1 (b_1 + b_{12} C_2 + 2 b_{11} C_1)}{1 + b_1 C_1 + b_2 C_2 + b_{12} C_1 C_2 + b_{11} C_1^2 + b_{22} C_2^2} \tag{5}$$

$$q_2 = \frac{q_s C_2 (b_2 + b_{12} C_1 + 2 b_{22} C_2)}{1 + b_1 C_1 + b_2 C_2 + b_{12} C_1 C_2 + b_{11} C_1^2 + b_{22} C_2^2} \tag{6}$$

In some cases, Eqs. (5) and (6) can be simplified

by reducing the number of parameters. In the case of single compound isotherms, only the parameters relevant to this compound are needed.

It is important to point out at this stage that all these isotherm models are competitive, meaning that the amount of compound *i* adsorbed at equilibrium with a solution of constant concentration C_i decreases with increasing concentration C_j of any other adsorbed component of the solution. There are few exceptions to this rule in the literature. As we will show later (see Section 4.2), the case in point, Tröger's base enantiomers on Chiralpak AD, turns out to be one of them. The simpler interpretation of our experimental results (see Section 4.2) is by assuming multi-layer adsorption or a relatively high degree of adsorbate adsorbate association on the surface of the stationary phase [37]. Accordingly, a modified isotherm model is applied that accounts for both the S-shape of the adsorption isotherm of the more retained compound and for the unusual positively cooperative adsorption behavior of the less retained compound:

$$q_1 = \frac{b_a C_1 (q_{max} - k_2 C_2)}{1 + b_a C_1} + \frac{k_2 b_b C_1 C_2}{1 + b_b C_1} \quad (7)$$

$$q_2 = \frac{q_s C_2 (b_2 + 2 b_{22} C_2)}{1 + b_2 C_2 + b_{22} C_2^2} \quad (8)$$

This isotherm model assumes that there are two different binding sites for the less retained compound on the surface of the CSP, with a maximum saturation capacity q_{max}. However, this first enantiomer can interact directly only with the first binding site. In the absence of the more retained enantiomer, its isotherm reduces to a Langmuir isotherm (first term in Eq. (7)). When both enantiomers are present in a mixture, the second site is occupied by the more retained enantiomer and an association between the CSP and molecules of both enantiomers is formed. Therefore, the less retained compound has a higher adsorption capacity in the presence of the second enantiomer than without it. The distribution between these two sites is strongly dependent on the concentration of the two compounds. The binary adsorption becomes cooperative instead of being competitive as it usually is. The isotherm model of the more retained compound accounts for the inflection point observed. It does not take into account a possible influence of the less retained enantiomer on its adsorption. For this compound, a noncompetitive isotherm model is applied. If there is competition or cooperation, its intensity is too small to be significant. More detailed information regarding the experimental data which define this isotherm model is given later (see Section 4.2).

2.3. Revised set of separation conditions

The successful operation of an SMB process relies on the fulfillment of a number of separation conditions. To achieve a good separation, the flow-rates in all four sections must be chosen in such a way that the fronts and rears of the bands of the two components of the feed are within specific location ranges at the end of each cycle. Ruthven and Ching [9] showed that an SMB separation can be studied as an equivalent TMB process when the simulated solid-phase flow-rate of the SMB system is identical to the solid-phase flow-rate of the TMB process. This flow-rate is given by:

$$Q_S = (1 - \epsilon_k) A u_s = (1 - \epsilon_k) A L_C / t^* \quad (9)$$

where t^* is the switching (or cycle) time, u_s the apparent velocity of the solid phase, and *A* the cross section area of the column. The internal flow-rate of the TMB can be calculated by using the relationship:

$$Q_j^{TMB} = Q_j^{SMB} - Q_S / F_k \quad (10)$$

The derivation of the separation conditions is based on the ideal or equilibrium model, i.e., on the assumption that the contributions of axial dispersion and the mass transfer resistance to band broadening are all negligible and that the column efficiency is infinite. In conventional studies of SMB, it is further assumed that the solid phase flow-rate through each column and the void fraction of each column are the same. In a previous publication [19], we introduced a revised set of separation condition which takes into account the fact that the columns of an SMB set have each a different porosity. When the columns ($k = 1, \ldots, n$) of an SMB have different properties, the true period of the system, i.e., the time after which the system returns to its initial conditions, is no longer the switching time but is *n* times larger. We call this time the superperiod of the SMB. As

explained earlier, we focus in this work on the effects arising from columns having different porosities, hence different retention factors for the components of the feed. The retention factor of component i in the physical column k (column which will be successively part of the four different sections of the SMB) is proportional to the Henry coefficient, a_i, and to the phase ratio, F_k. Thus, the exact values of these important design parameters will vary from column to column. Every column leads to a different set of separation conditions and the number of these conditions equals the number of columns in the SMB process considered. Obviously, the characteristics of the production (amount produced per cycle and purity of both output streams) will vary during a superperiod. Based on the so called ''triangle theory'' [11–13], the derivation of a revised set of separation conditions chooses the flow-rates through the four sections of an SMB process and takes into account the characteristics of the different columns used. By defining the dimensionless internal flow-rate ratios as:

$$r_j = \frac{Q_j t^*}{AL_C} \tag{11}$$

we can extend the conventional separation conditions [11,12]. These flow-rate ratios do not depend on the column porosities. By contrast, the following boundary parameters consider the column porosities:

$$g_k = a_1(1 - \epsilon_k) + \epsilon_k \tag{12}$$

$$h_k = a_2(1 - \epsilon_k) + \epsilon_k \tag{13}$$

In these equations, the subscript k identifies the physical column. A simple algebraic transformation [19] leads to the following new set of equations under linear conditions:

$$r_I \geq h_k \tag{14}$$

$$g_k \leq r_{II} \leq r_{III} \leq h_k \tag{15}$$

$$r_{IV} \leq g_k \tag{16}$$

Thus, the operating conditions, which are described by the four internal flow-rates, do not change depending on the subset of physical columns contained in the section considered during a given cycle. Only the boundaries of the inequalities which define the conditions to be satisfied by the r_j values are functions of a_i and ϵ_k. These boundaries depend on the specific columns considered. Thus, when the columns are different, there is a different operating triangle in the (r_{II}, r_{III}) plane for each column. To achieve complete separation, based on the equilibrium theory [10], the operating conditions must be chosen in such a way that the corresponding point in the (r_{II}, r_{III}) plane is located inside all of these triangles, defined by the parameters of the separation. Since the production rate depends on the location of the point inside the triangle, variations between the column characteristics will cause a certain decrease in the production rate of the unit considered. The revised separation conditions also can be extended to nonlinear separation conditions, at least in the case of a Langmuirian adsorption isotherm [38].

3. Experimental setting

3.1. Chemicals, solvents and columns

The racemic mixture of Tröger's base (Aldrich, Milwaukee, MI, USA) was separated using chromatographic columns packed with Chiralpak AD from Chiral Technologies (Exton, PA, USA). Tröger's base (see Fig. 2) has a molecular mass of 250.35 g/mol. The purchased sample was only 98% pure (as determined by gas chromatography). In order to measure accurate isotherm data, it was necessary to purify this mixture. This was done by overloaded elution chromatography on a C_{18} silica packing material, in a 5 cm I.D. axial compression column [39] and by crystallization [38]. Fig. 3

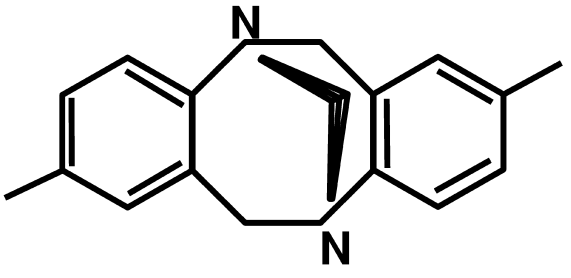

Fig. 2. Structure of Tröger's base.

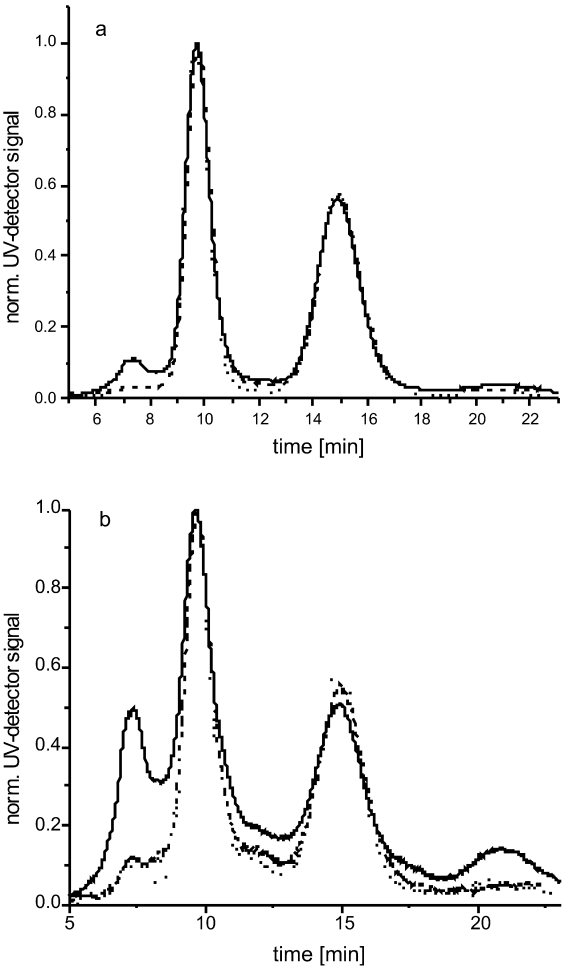

Fig. 3. Comparison of the composition of the original (Aldrich) and the purified Tröger's base mixtures: analytical injection at a wavelength of 308 nm (a) and 315 nm (b) Solid line – original product, dashed line – product purified by crystallization, and dotted line – product purified by separation on an axial compression column packed with C_{18} silica.

compares the compositions of the initial sample and of the two purified products. It demonstrates the superiority of the first purification method in the present case. Yet, the first eluted impurity was not entirely eliminated from the product used in this work. The mobile phase was pure HPLC-grade isopropanol from Fisher Scientific (Pittsburgh, PA, USA). It was used without further purification.

The stainless steel columns used in the experiments were of 10 cm×1 cm I.D. They were packed

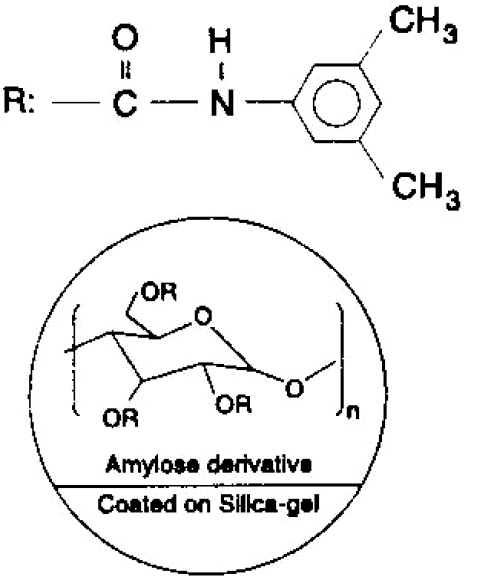

Fig. 4. Chemical structure of Chiralpak AD [40].

at Chiral Technologies, with Chiralpak AD, a silica-based packing material coated with amylose tri-(3,5-dimethyl carbamate), Fig. 4. The particle size is 20 μm. Chiralpak AD is widely used for the separation of compounds with aromatic, amides, carbamate, or ester groups, alkyl amines, and compounds with multiple chiral sites [40].

3.2. SMB system

A laboratory-scale SMB unit (ICLC 16-10) from Prochrom (now Novasep, Nancy, France) was used in an eight-column configuration. Five 16-port pneumatically-actuated valves (Valco, Houston, TX, USA) realize the continuous operation of the SMB process by switching the column position of the two inlet streams (solvent and feed) and the three outlet streams (extract, raffinate, and recycle). Constant flow-rates in the four sections are maintained using four HP 1050 pumps (Agilent Technologies, Palo Alto, CA, USA). This system is a so-called open SMB system since it has no additional pump for returning the recycle stream directly back into the flow cycle. The recycle stream is indirectly pumped back into the flow cycle together with the solvent stream.

Two Spectroflow UV detectors (Model 757 from

Perkin-Elmer, Foster City, CA, USA) monitor the composition of the extract and raffinate outlet streams. A HP 1100 UV detector (Agilent Technologies) with a high-pressure flow cell and a laser polarimeter (PDR-Chiral, Palm Beach Gardens, FL, USA) are installed within the flow cycle of the SMB system, at the outlet of one of the columns (see Fig. 1). Due to the switching of the outlet and inlet stream positions the detectors are shifted within the SMB scheme, at each cycle, and, accordingly, monitor the composition of the stream at this particular node, at its successive positions. The location of the two detectors was changed between experimental runs to record the concentration profiles at different column outlets. The UV flow cell and the polarimeter flow cell can be operated up to 600 bar and 460 bar (6000 p.s.i.; 1 p.s.i. = 6894.76 Pa), respectively. The experimental data from these four detectors are recorded using LabView (National Instruments, Austin, TX, USA), a program installed on an additional computer. The main computer, interfaced with the SMB, controls the SMB process by regulating the flow-rates, the switching time, and the setting of the five valves, using Chrosoft, a software package from Prochrom (now Novasep). A HP 1090 liquid chromatograph (Agilent Technologies) and its data acquisition system HP ChemStation were used to determine the characteristics of each column of the SMB, the adsorption isotherm parameters of the CSP, and the purities of the extract and the raffinate streams during each run.

3.3. Calculation of the single concentration profiles

The response factors of (nonchiral) UV detectors to both enantiomers are equal. Those of (chiral) polarimeters are equal in absolute value but opposite in sign. In principle, the concentration profiles of two enantiomers can be calculated simply, by combining the signals of a UV detector and a polarimeter located one immediately after the other, as they are in our instrument. To obtain the single component profiles, however, accurate and precise calibrations of the two detectors are required. The UV detector response at the wavelength of 308 nm is only slightly nonlinear over the concentration range investigated. Therefore, the calibration curve can be fitted by the following function:

$$C = C_R + C_S = a\mathrm{UV} + b\mathrm{UV}^2 \tag{17}$$

The response of the polarimeter remains linear in the same concentration range, hence:

$$C_R - C_S = \frac{[\alpha]}{[\alpha]_0 l} \tag{18}$$

Subtracting Eq. (18) from Eq. (17) gives the concentration of the enantiomer C_S with the negative optical rotation, as:

$$C_S = \frac{1}{2} \cdot \left(a\mathrm{UV} + b\mathrm{UV}^2 - \frac{\alpha}{[\alpha] l} \right) \tag{19}$$

with a similar equation to calculate C_R. Note that this procedure leads to a systematic error whenever the stream contains impurities that are detected by either the UV spectrophotometer or by the polarimeter. The most frequent case is when the sample contains impurities that absorb UV light at the wavelength used (see next section). Also it is worth noticing that, to reduce the response of the analytical detectors, the wavelength at which the three UV detectors are operated were chosen on the sharp front of the UV spectrum. Due to the different UV spectra of the racemic mixture and the impurities, using several different UV detectors under these conditions can introduce additional errors into the data analysis.

4. Results and discussion

4.1. Column characteristics

The determination of the characteristics of the columns used was the first step of this study. Successively, 25 μl samples containing low concentrations of a nonretained compound (1,3,5-tri-*tert*.-butylbenzene) and of the racemic mixture were injected onto nine columns, at a flow-rate of 1 ml/min. In Table 1 the retention volumes of the nonretained compound and of both enantiomers are reported. These volumes are the average of four repeated measurements. The maximum relative standard deviation (RSD) of the measurements made on one column was less than 0.025% for the non-

Table 1
Characteristic parameters of the columns used

Column	Position in SMB	V_0 (ml)	V_1 (ml)	V_2 (ml)	k'_1	k'_2	Porosity, ϵ	Phase ratio, F
c04*		5.144	9.830	14.720	0.912	1.861	0.648	0.543
c14	7	5.193	9.833	14.405	0.894	1.773	0.654	0.528
c11	5	5.169	9.844	14.400	0.906	1.785	0.651	0.528
c12	6	5.163	9.781	14.255	0.895	1.761	0.650	0.538
c13	8	5.170	9.796	14.495	0.895	1.805	0.651	0.535
c09	4	5.123	9.752	14.410	0.904	1.869	0.645	0.550
c05	2	5.119	9.857	14.629	0.925	1.859	0.645	0.551
c02	1	5.104	9.835	14.827	0.927	1.903	0.643	0.556
c08	3	5.094	9.750	14.250	0.915	1.801	0.642	0.559
Average value		5.142	9.806	14.496	0.908	1.820	0.648	0.543
Standard deviation (SD)		0.036	0.042	0.210	0.013	0.051	0.004	0.012
RSD (%)		0.705	1.450	1.450	1.473	2.811	0.680	2.284
Defect	6	4.917	9.30	13.00	0.90	1.81	0.619	0.615

*Column used in the HP1090 system to determine the adsorption isotherm parameters and the purity values of the outlet streams.

retained compound. From these three retention volumes, the retention factors k' of the two enantiomers, the porosity of the column and its phase ratio were calculated. Although the columns had been carefully packed, the RSD of the nine phase ratios is still 2.3% (Table 1). This parameter has an significant influence on the solution of the mass balance Eq. (1) (see Section 2.1). In Table 1 the position of the eight columns in the SMB unit are listed. The column c04, which has the same porosity as the average value of all the columns, was used to determine the adsorption isotherm parameters. During this experimental study the retention volume of the non-retained compound on this column was frequently checked to assess the integrity of the column. No measurable change in this retention volume was ever observed. Fig. 5 compares three analytical injection profiles. Two of these profiles were calculated from the values of the Henry coefficients of the Tröger's base enantiomers, using the maximum and the minimum porosity values in the regular set of columns (dotted and solid lines, respectively). Note how strongly the retention time of the more retained compound depends on the applied porosity. Due to the different adsorption behaviors of the two enantiomers the influence on the retention time is more significant for the more retained compound. The difference between the two extreme retention times for the columns in the regular set is approximately 18 s. For the less retained compound, this difference is only 5 s. These results are in agreement with the experimental data in Table 1. There was also one ''defective'' column that was specially packed for this purpose. It has a low porosity and the retention times observed are noticeably different. The dashed line in Fig. 5 represents the chromatogram calculated for this column, which has a total porosity of 0.619.

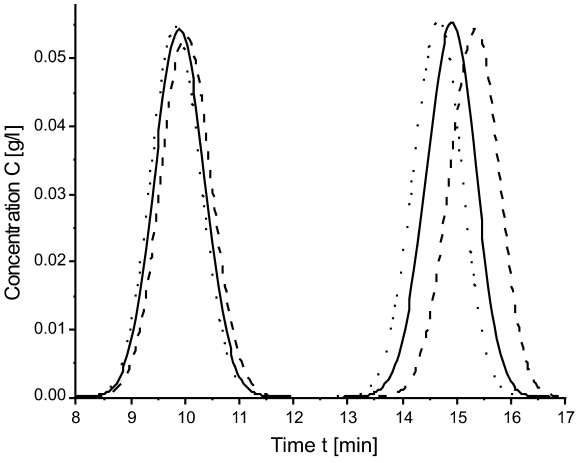

Fig. 5. Calculated profiles of elution bands obtained upon analytical injection into columns with different porosities, at a flow-rate of 1 ml/min. Solid line – smallest porosity value, $\epsilon = 0.642$, dotted line – largest porosity value, $\epsilon = 0.654$, and dashed line – ''defective'' column, $\epsilon = 0.619$.

Table 1 reports also the retention times and characteristics for this column. The respective differences between the retention times of the less and the more retained enantiomers with the defective column and their average retention times on the nine well-packed columns are 9 and 36 s, respectively.

Finally, before investigating the behavior of the SMB process with these column, we had to measure the adsorption isotherm parameters of the enantiomers in the system selected. The unusual but interesting adsorption behavior of Tröger's base on ChiralPak AD is described in detail in the following section.

4.2. Estimation of adsorption isotherm

Although it was attempted, it proved impossible to determine the adsorption isotherm of these two enantiomers by frontal analysis (FA). In spite of several attempts at the purification of the racemic mixture purchased by crystallization or by preparative chromatography, the unidentified impurities could not be eliminated entirely. Fig. 3 compares the composition of analytical-size samples of the racemic mixture, before and after purification, at two different wavelengths, 308 and 315 nm. The mixture could be well cleaned from the first impurity but the remaining impurities still influenced slightly the retention times of the breakthrough profiles in FA. Therefore, the perturbation method was applied as an alternative (see Ref. [37] for more detail).

Compared to the FA method, the perturbation method does not require the accurate calibration of the UV detector but it does require the selection of an adsorption isotherm model in order to analyze correctly the experimental data acquired. Following the equilibrium theory, only the retention volumes (or times) of perturbations traveling through the chromatographic column are measured. The column is equilibrated with a stream of solvent containing a known concentration of a mixture of the two enantiomers. Perturbations are created by the injection of a sample amount small enough to cause but a minor perturbation of the equilibrium between the two phases in the column. The number of perturbation peaks observed depends on the number of components dissolved in the mobile phase. Each component affects each characteristic retention volume. The method is explained in more detail elsewhere [30,37,41–44].

Plots of the retention times of the two perturbations versus the plateau concentration are shown in Fig. 6. This figure contains data measured using either the pure compounds or the racemic mixture. Both compounds exhibit an unusual adsorption behavior, both as pure compounds and in the racemic mixture. The less retained compound, (+)-Tröger's base, exhibits Langmuirian adsorption behavior when it is pure (monotonous decay) but a most unusual adsorption behavior when in the presence of the second enantiomer, indicating that the amount adsorbed at equilibrium increases with increasing concentration of both enantiomers, suggesting cooperative adsorption behavior (Fig. 6). Such an adsorption behavior is the opposite of the classical competitive behavior that causes the displacement effect usually observed in chromatography. The isotherm model that was adopted (see Eq. (7) and was introduced earlier, in Section 2.2), accounts for this behavior. The retention times of the perturbations corresponding to the more retained enantiomer

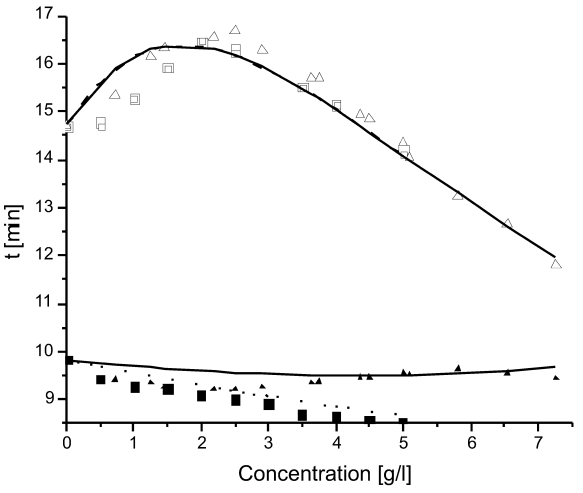

Fig. 6. Comparison of the retention times of perturbations measured (symbols) and calculated from the best adsorption isotherm model (lines): Solid square – single (+)-Tröger's base, empty square – single (−)-Tröger's base, solid triangle – first retention time of the racemic mixture, empty triangle – second retention time of the racemic mixture, solid line – racemic mixture of Tröger's base, and dotted line – single (+)-Tröger's base [note: same model for single compound and mixture of (−)-Tröger's base].

have a maximum value, corresponding to an inflection point of the isotherm, which is, thus, S-shaped (see Fig. 6). This adsorption behavior is accounted for by the quadratic isotherm model (see Eq. (8)).

Using the Marquardt–Levenberg iteration procedure [45], the set of measured perturbation retention times was fitted to the theoretical retention times based on the isotherm model and best values of its parameters were determined. These parameters are reported in Table 2. The lines in Fig. 6 show the values of the retention times of the pulses obtained by injecting samples of the pure compounds or the mixture (dashed and solid lines, respectively) which are derived from the isotherm model and these parameters [37]. These lines are in excellent agreement with the experimental data (symbols). In order to validate further this adsorption isotherm model, overloaded band profiles were calculated and compared to the experimental chromatograms for the injection of a 1 ml sample containing 14.5 g/l of Tröger's base. The two chromatograms in Fig. 7 show also excellent agreement, both for the retention times and the peak-profile shapes. Finally, Fig. 8 compares the adsorption isotherm determined by the perturbation method to the experimental data obtained by FA. The two sets of experimental isotherms differ slightly. This difference is caused by the presence of impurities in the sample (see earlier). These impurities cause systematic errors in the calibration of the UV detector, hence discrepancies in the estimates of the amounts adsorbed at equilibrium. However, similar trends are found in the two sets of data determined by FA and by the perturbation method. The theoretical work of Biressi et al. [46], showed that the ''triangle theory'' cannot be solved analytically for convex downward (e.g., anti-Langmuirian) isotherms. In an attempt to use this theory, the adsorption data obtained for the two enantiomers of Tröger's base were fitted to the

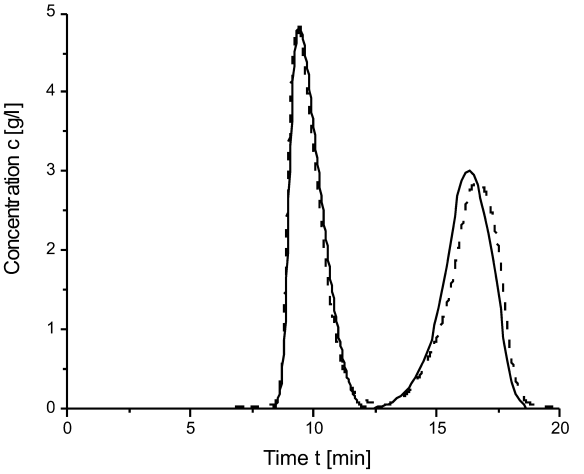

Fig. 7. Calculated and experimental overloaded elution profiles, illustrating the validity of the isotherm model: solid line – calculated profiles; dashed line – experimental profiles.

Table 2
Best values of the parameters of the adsorption isotherm models

Cooperative and S-shaped adsorption isotherm

q_{max} (g/l)	b_a (l/g)	b_b (l/g)	k_2 (l/g)	q_s (g/l)	b_2 (l/g)	b_{22} (l^2/g^2)
54	0.0311	−0.03618	−0.7319	27	0.1269	0.01532

Best fit competitive Langmuirian adsorption isotherm

q_s (g/l)	b_1 (l/g)	b_2 (l/g)
335.8	0.0005	0.01251

Competitive Langmuirian adsorption isotherm with analytically determined Henry coefficients

q_s (g/l)	b_1 (l/g)	b_2 (l/g)
54	0.0311	0.06344

Initial slope of the adsorption isotherm

a_1	a_2
1.679	3.246

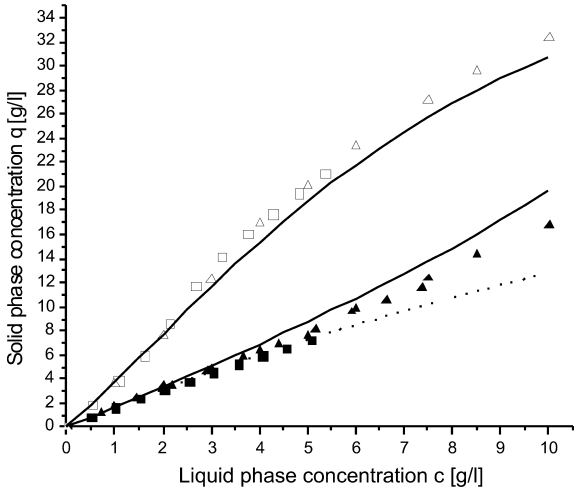

Fig. 8. Comparison of the adsorption isotherms determined by the perturbation method and the experimental data measured by frontal analysis (FA): solid square – FA single (+)-Tröger's base; empty square – FA single (−)-Tröger's base; solid triangle – FA based on the first retention time of the racemic mixture; empty triangle – FA based on the second retention time of the racemic mixture; solid line – racemic mixture of Tröger's base; and dotted line – single (+)-Tröger's base (note: the same models are used for single compounds and for the racemic mixture of Tröger's base).

classical competitive Langmuir model (Eq. (4)). An r^2 value of 0.997 was obtained. However, the best values obtained for the Henry coefficients, a_1 and a_2, were found to differ markedly from those measured on analytical chromatograms (see Table 2 and Fig. 3), rendering the results of this calculation useless. Therefore, the data were fitted again with the constraint that the Henry coefficient were to be equal to the experimental value. Although the result of the fit exhibited a better agreement in the low concentration range, large deviations were observed at high concentrations and the r^2 value was only 0.835. The model parameters are summarized in Table 2.

4.3. SMB experiments

4.3.1. Determination of the separation area

The separation area can be determined from the column characteristics and the parameters of the isotherm model. This area is easily calculated under linear separation conditions, according to the equilibrium theory. Under nonlinear conditions, it may be determined analytically only for the competitive Langmuir isotherm [10,46]. For all other adsorption isotherm models, the equations of the ideal model must be solved numerically. As an alternative, the entire region of $r_{II} - r_{III}$ was scanned by solving the mass balance equations (Eq. (1)) with their initial and boundary conditions for the SMB process, using, for the sake of fast numerical calculations, the conventional forward–backward finite differences algorithm [30]. This calculation supplied the purity of the extract and the raffinate streams as functions of the two flow-rate ratios.

The results of this computational scanning are illustrated in Fig. 9 for a purity of at least 98% of both outlet streams. The total feed concentration of Tröger's base was 7 g/l. For this scanning, a number of theoretical plates equal to 150 plates was assumed for each column. This number corresponds to a total of approximately 1200 plates for the eight-column train. The flow-rate ratios in sections I and IV were kept constant ($r_I = 2.1$ and $r_{IV} = 1.2$) but those for sections II and III were changed systematically within their boundaries. The values for r_I and r_{IV} were chosen based on the Henry coefficients. As an additional constraint a practical minimum flow-rate

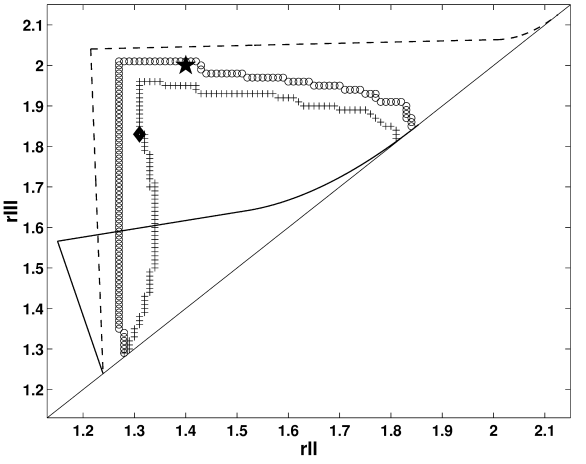

Fig. 9. Separation region under nonlinear condition (average 98% purity): solid line – competitive Langmuir isotherm with correct analytical Henry coefficients; dashed line – best competitive Langmuir isotherm based on Eq. (4); o-boundary – calculated for $\epsilon_{av} = 0.648$ (98% purity); +-boundary – calculated for ϵ_{exact} porosity both boundaries based on Eqs. (7) and (8) (isotherm parameters see Table 2). Experimental operating points, ★ – operating point 1 and ◇ – operating point 2.

must be considered, the flow-rate at which the pumps cannot reliably deliver a solvent stream. The switching time of 940 s was chosen to minimize the pressure differences in the SMB system which reduced the influence on the polarimeter signal.

The results of the calculations carried out using the average porosity value ($\epsilon_{aver}=0.648$) of the column set, as usually done in practical applications of computer modeling of SMB, predict that operating the SMB under experimental conditions within the area limited by the lines marked by the ◦ symbols affords a purity of 98% or better for both outlet streams. A significant influence of the nonlinear behavior under these separation conditions can be observed by comparing this area and the one limited by the dashed line. When the calculations are made with the exact values of the porosity of each of the eight column, however, the 98%-purity separation area (within the lines marked with the + symbols) shifts significantly downward. In this last calculation, the purities of the two outlet streams were averaged over one superperiod and compared to the minimum constraint (98%) to determine the area border. The comparison of the two separation areas shows that column-to-column fluctuations causes a significant loss in separation area and, more importantly, in potential production rate. The separation areas corresponding to both competitive Langmuir isotherm models mentioned earlier (Eq. (4)), the best fit and the fit with the correct Henry coefficients, are also drawn in Fig. 9, with dashed and solid border lines, respectively (see Table 2). The comparison of these last two separation areas with those calculated above illustrates the importance of an accurate determination of the adsorption isotherm and of its correct modeling. Not even the linear model, which uses only the correct Henry coefficients, could give a good estimate of the actual separation area. As expected, it overestimates the separation area and the production rate.

The isotherm model used was validated by operating the SMB under the experimental conditions corresponding to two operating points within the separation region and comparing experimental and calculated performance. The first operating point (symbol ★) lies close to the upper ◦ symbol boundary of the separation area. Under the corresponding set of conditions, the purity should be better than 98% if the calculations made with the average porosities is correct but not if the influence of the differences in porosities of the columns are taken into account. The second operating point (symbol ◇) is in the ''safe'' region of the separation area, when the calculations are made with the average porosity value, a region where both outlet streams should be pure. However, this point lies on the + symbol boundary of the separation area, as calculated using the exact porosity values. By operating under the conditions corresponding to this last point and substituting the defective column to a good one (position 6), the influence of the homogeneity of the column set on the stability of the process could also be studied.

Finally, another useful validity check of the isotherm model can be made, a comparison between the experimental and calculated concentration profiles of the two enantiomers along the column train of the SMB. The experimental determination of these profiles requires a proper calibration of the two detector signals, in order to calculate the concentrations of the two enantiomers profiles from the combination of the signals of the UV detector and laser polarimeter.

4.3.2. Results at operating point ★

Once the separation area of the experimental system has been defined, the SMB process can be started. The first set of operating conditions selected is close to the upper boundary of the separation area for a solution of 7 g/l *rac*-Tröger's base. The dimensionless flow-rate ratios (Eq. (11)) for sections II and III are 2 and 1.4, respectively. The switching time must be adjusted for the dead volumes of 0.31 ml between the columns, depending on the flow-rates in the middle sections. Using the average porosity value, the operating point should lie within the 98% boundaries of the separation area. If the exact porosity values are used in the calculations, however, the operating point lies outside these boundaries. Fig. 10 shows the conventional concentration profiles of the extract and the raffinate streams during the start-up period. The duration of this period can be clearly identified, although, in principle, the process reaches steady state only asymptotically. The superperiod can also be observed under the operating conditions described above. This is particularly clear for the raffinate stream (black line), although it can be seen

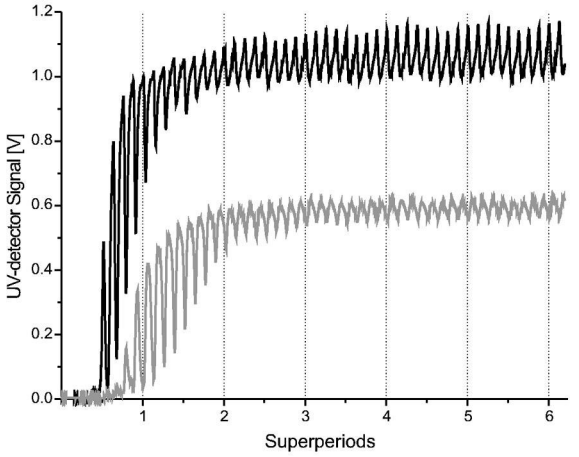

Fig. 10. UV detector signals for the extract (gray) and the raffinate (black) outlet streams.

also for the extract stream (grey line). The superperiod lasts eight cycles, after which the profiles return to their original shape. As explained earlier, the composition of the stream at the exit of one column, shifting from node to node in the SMB scheme during a superperiod, was monitored. Fig. 11 shows the record of the UV detector signal (total concentration of Tröger's base) and Fig. 12 that of the polarimeter signal [excess of (+)- over (−)-Tröger's base]. Using this online monitoring system, the concentration profiles along the column train, or rather the elution profiles at one node during a superperiod, can be derived. There are four lines in the figures. The top two lines (which are very close) show the signals recorded when the UV detector is located at the outlet of column in positions 7 (dash–dotted lines) and 6 (dotted line). They show a slight shift of the fronts toward the desorber exit when the node moves from position 6 to 7. This shift explains the origin of the slow oscillations of the maximum of the outlet stream concentration (see Fig. 10). The lower two lines were both calculated for the node in position 6, assuming the average porosity of the column train (solid line) and using the exact porosities (dashed line).

An excellent agreement is observed between the positions of the concentration fronts of the experimental and calculated concentration profiles in sections II, III, and IV of the SMB. This agreement extends to the existence and positions of small oscillations on the concentration plateaus. These observations validate the isotherm model used. There

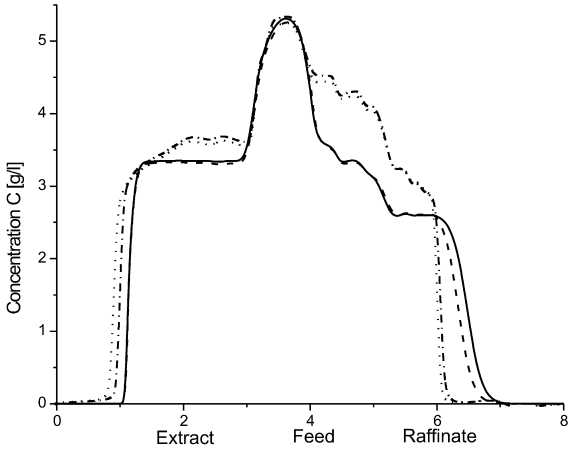

Fig. 11. Internal concentration profiles for the first operating point (★) measured at the column outlet by the UV detector over one superperiod (eight cycles): dash–dotted line – experimental UV signal at position 7, dotted line – experimental UV signal at position 6, solid line – profiles calculated with the average porosity value, dashed line – profiles calculated at position 6 with the exact porosity values.

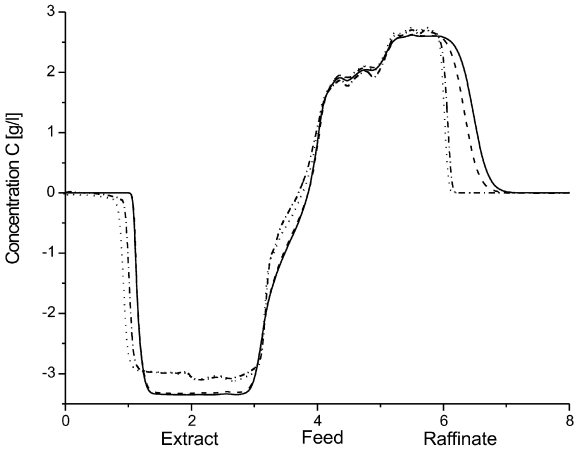

Fig. 12. Internal concentration profiles for the first operating point (★) measured at the column outlet by the laser polarimeter over one superperiod (eight cycles): dash–dotted line – experimental polarimeter signal at position 7, dotted line – experimental polarimeter signal at position 6, solid line – profiles calculated with the average porosity value, dashed line – profiles calculated at position 6 with the exact porosity values.

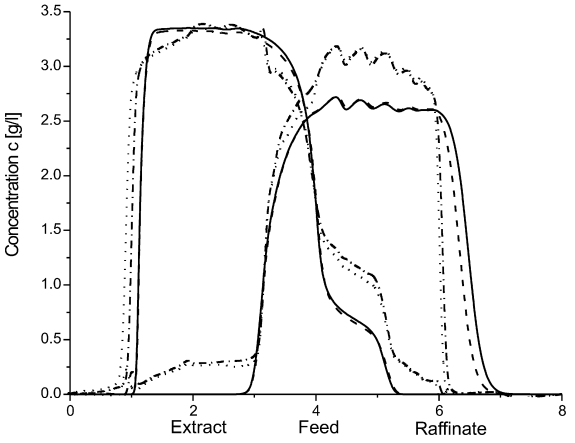

Fig. 13. Internal concentration profiles for the first operating point (★) determined at the column outlet by combining the UV detector and the laser polarimeter signals over one superperiod (eight cycles): dash–dotted line – experimental signals at position 7, dotted line – experimental signals at position 6, solid line – profiles calculated with the average porosity value, dashed line – profiles calculated at position 6 with the exact porosity values.

are significant differences between the heights of these profiles, however, particularly in positions 3, 5, and 6. All concentrations in Fig. 11 tend to be higher for the experimental profiles, especially in the middle sections. In Fig. 12 the differences between experimental and simulated profile heights cannot be observed. The reason of this difference is apparent in Fig. 13 which shows the individual concentration profiles of the two enantiomers derived from Eq. (19) and its analog. These profiles should be compared to the total concentration profiles shown in Fig. 11. The difference between the experimental and calculated concentration profiles can be identified as due to the accumulation of the feed impurities in the middle section of the SMB. The polarimeter does not detected these impurities that are nonchiral. The presence of these impurities is further verified by the results of the analysis of the two outlet steams collected over the time of one superperiod. No raffinate is detected in the extract stream but some amount of impurities is observed. The raffinate stream contained 1.5% and 1.8% of extract during two different runs made under the same experimental conditions. It also contained approximately 5% impurities, which confirms the experimental profiles in Fig. 13. Unfortunately, these impurities could not be quantified because we were not able to isolate a sufficient amount of them to calibrate the detectors for them.

Due to the presence of these impurities, the calculated values of the production rate of the SMB process at this operating point and of the purity of the outlet streams cannot be compared directly to the experimental results. Therefore, Table 3 compares only the computed values to show the influence of the porosity on the purity and the production rate. The experimental conditions are the same as those described earlier. Again, the extract stream contains no raffinate, in agreement with the experimental results. The amount of extract produced remains the same for each cycle. By contrast, the purity of the raffinate varies from cycle to cycle. The difference between its compositions calculated using the average porosity values or using the exact porosity of each column and averaging the purity of each cycle is nearly 1% (0.83%). The production rate of the raffinate stream is larger by (3.03%) when calculated from the exact column porosities.

Table 3
Purity and productivity of the extract and raffinate streams simulated for the first operating point ★

	Purity		Productivity	
	Extract	Raffinate	Extract, 10^{-4} mg s^{-1} ml^{-1}	Raffinate, 10^{-4} mg s^{-1} ml^{-1}
Values when using ϵ_{aver}	99.97	98.03	7.51	8.88
Averaged values when using exact ϵ	99.84	96.89	7.31	9.27
Difference	0.13	1.14	0.2	0.39
RSD (%)	0.09	0.83	1.92	3.03

4.3.3. Results at operating point ◇

The second operating point was chosen to correspond to more robust experimental conditions within the separation area using the average porosities. The values of the dimensionless flow-rate ratios in sections II and III are 1.3 and 1.83, respectively. The raffinate stream should be pure, which is confirmed by the experimental results. All the analytical samples of the raffinate stream collected over a superperiod are pure of extract. Small amounts of raffinate (approximately 1%) were detected in the extract stream. Impurities were also detected in both streams. Again, more precise figures cannot be given for the reason explained in the previous section and limitations of the data acquisition system. The experimental concentration profiles of both enantiomers are displayed in Fig. 14. In this experiment, the profiles were successively recorded at three different column outlets (by moving the detectors from one node to the next). The dash–dotted, dash–dot–dotted, and dotted lines represent the concentration profiles passing at the node immediately downstream of columns 8, 7, and 6, respectively. A significant shift of the front positions can be observed as in the previous case. The positions of the fronts of the experimental and calculated profiles do not agree as well as in the previous case (see Fig. 15). Now, the impurities accumulate in the central sections and this may cause the shift of the fronts observed by influencing the adsorption behavior of the two enantiomers. However, the calculated profiles show similar oscillations as seen in the experimental profiles. The location of the calculated fronts on the extract side shifts depending on the porosity values used.

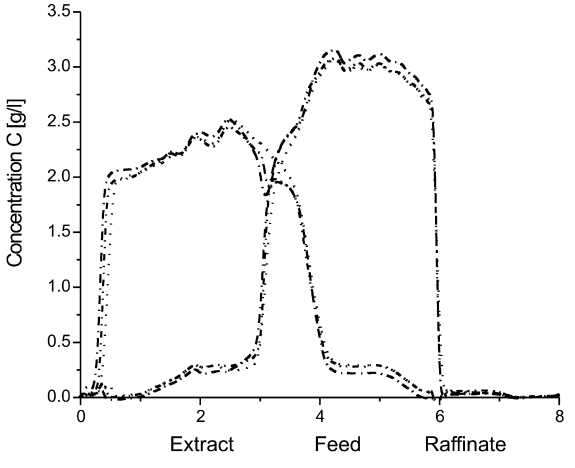

Fig. 14. Experimental internal concentration profiles for the second operating point (◇) determined at the column outlet by combining the UV detector and the laser polarimeter signals over one superperiod (eight cycles): dotted line – signals at position 6, dash–dot–dotted line – signals at position 7, and dash–dotted line – signals at position 8.

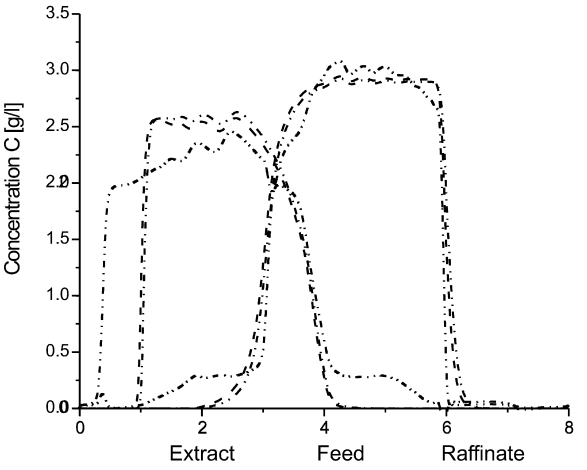

Fig. 15. Internal concentration profiles for the second operating point (◇) determined at the column outlet by combining the UV detector and the laser polarimeter signals over one superperiod (eight cycles): dash–dot–dotted line – experimental signal at position 7, solid line – profile calculated with the average porosity value, dashed line – profiles calculated at position 7 with the exact porosity values.

4.3.4. Operating of the SMB with a defective column

In a last experiment, we investigated the influence of a defective column on the performance of the SMB process. One of the columns (position 6) was replaced with a column having a porosity markedly lower than average, 0.619 instead of 0.648. The characteristics of this column are given in Table 1. The same operating conditions are kept as for the previous operating point ◇. In Fig. 16, two experimental concentration profiles (dash–dot–dotted – position 6 and dash–dotted – position 5) are compared to the profiles calculated with the average porosity (solid line) and with the exact values of the column porosity (dotted – position 6 and dashed –

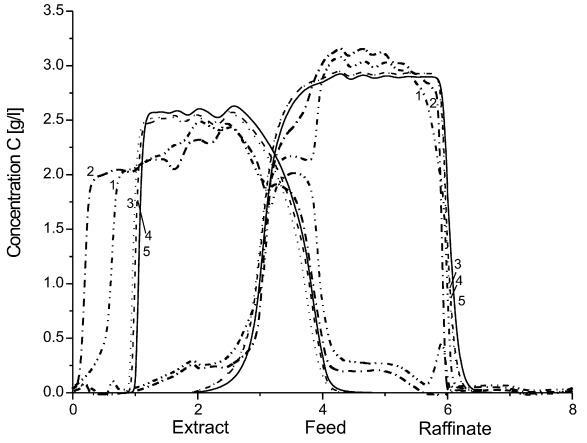

Fig. 16. Internal concentration profiles for the second operating point (◇) with the ''defective'' column in position 6, measured at the column outlet by combining the UV detector and the laser polarimeter signal over one superperiod (eight cycles): dash–dot–dotted line (1) – experimental signal at position 6, dash–dotted (2) line – experimental signal at position 5, solid line (5) – profile calculated with the average porosity value, dotted line (3) – profile calculated at position 6 with the exact porosity values, dashed line (4) – profile calculated at position 5 with the exact porosity values.

position 5). A shift of the calculated profiles at least as large as the one observed for the operation point ◇ is observed. In addition, a significant change in the steepness of the experimental front of the raffinate profile is observed when the detectors are located at the outlet of the defective column. The fronts of the extract band of the experimental and calculated profiles are closer to the beginning of section I, especially when recorded or calculated at the outlet of the defective column.

Again, due to the present of the impurities and their influence on the UV detector calibration the calculated and simulated results cannot be compared directly. In all outlet streams we detected traces or even larger amounts of the impurities. In addition, the extract stream was polluted with approximately 1% raffinate.

These results illustrate the considerable advantage of using an online monitoring system. The combination of the response of the two detectors gives immediate notice of any significant changes of the band profiles, hence, e.g., of a drift of the column characteristics. With the help of a simple program controlling the data acquisition system, the real time concentration profile can be compared continuously to previous profiles or/and calculated profiles. Significant deviations can trigger the issue of appropriate warnings. Also when the adsorption behavior of the feed components changes, the operating conditions of the SMB process can be re-adjusted to maintain the complete separation of the products.

5. Conclusions

The combination of a UV detector and a laser polarimeter allows the continuous monitoring of the composition of any outlet stream containing the two enantiomers and also that of the internal concentration profiles within the SMB unit. The results of this online monitoring method and the predictions of a suitable model of the SMB and of its column behavior can be incorporated into a process control system. The presence of impurities causes some manageable difficulties in the determination of the separation parameters and in the operation of the SMB process (especially because the presence of these impurities introduces a systematic error into the UV detector calibration). This study permits a detailed investigation of the separation process in SMB and improves our understanding of its operation under nonlinear conditions. From the theoretical and experimental studies reported here, we can derive the conclusions summarized below.

1. The SMB process is more complex than it seems, especially when used to separate compounds under nonlinear conditions. This process is influenced by numerous parameters, e.g., column properties, SMB system with its extra column volumes, presence of impurities, and adsorption isotherm parameters. Using the average values of the column characteristic parameters to calculate the concentration profiles and the composition history of the flux is a common simplification that reduces the number of operating parameters and the amount of computational time. However, the column properties as well as all other significant parameters should be considered to reach better agreement between simulated and experimental profiles.
2. The calculation of the optimum operating conditions of SMB is more complicated when the

separation is implemented for compounds exhibiting nonconventional isotherm behavior than for those whose adsorption follows the competitive Langmuir model. It is, however, possible by numerically scanning the separation area (Fig. 9). The effect of the nonlinear behavior of the isotherm is described easily using r_j (Eq. (11)) to define the separation conditions. When the isotherm is nonlinear and the feed concentration increases, the region of complete separation changes shape and size. Its boundaries are a curvilinear triangle. Shifts in the separation area arise when the porosity of the columns used is different. These shifts have significant impact on the choice of the operating point and on the production rate. In order to achieve high purities of both enantiomers produced, the operating point must be located inside the triangle corresponding to n identical columns having the average porosity but not too close to its apex or its borders. This condition arises from: (a) the need to use columns with a finite efficiency and (b) because all the columns have different properties, hence different separation areas.

3. Column-to-column fluctuations of the bed homogeneity adversely affects the robustness of the operating conditions near the optimum. The closer the process is operated to its optimum or boundaries, the more the production rate and/or the product purity decrease with increasing fluctuations of the column characteristics. The influence of variations of the column characteristics is more important under nonlinear conditions with nonlangmuirian adsorption behavior, as shown in our experimental study. However, no relationship indicating the allowable variation of a set of columns can be found as done under linear separation condition (see Fig. 4 in Ref. [19]). As shown in Fig. 9, using the exact porosity values during scanning provides an excellent tool for finding the accurate separation area. By applying the same separation constraints of 98% and better purity of both outlet streams, the purity simulated with the exact porosities averaged over one superperiod (as described in Section 4.3.1) changes its size in comparison to the averaged porosity value. In the case of a defect column in the SMB system, the separation area would change more significantly depending on the separation conditions and the porosity values.
4. Calculations and experimental results show that the separation area decreases with increasing amplitude of the column-to-column variations. Since the area of a separation triangle is already smaller under nonlinear than under linear conditions, the specifications regarding columns are most important in the case of difficult, nonlinear separations, as exemplified by the enantiomeric separation of the Tröger's base enantiomers discussed earlier. Although the fluctuation of the good columns was in an acceptable range (see Table 1), a significant change of the shape of the separation area can be observed (Fig. 9). Careful attention must be paid to setting and enforcing proper specifications for the acceptable range of variations of the column properties.
5. Increasing the number of columns in each section of the SMB unit dampens the effect of column-to-column fluctuations of any column characteristic [19]. However, the degree of dampening depends upon the specific system and its parameters. Especially, a unit with more than one column per section is more robust against an abrupt change of the packing density of one column during the separation process.
6. Although the characteristics of the columns used may be significantly different, the SMB unit still can separate two feed compounds successfully if their retention times differ sufficiently. An acceptable range of variation of column properties could easily be defined given appropriate constraints on the range of process performance by scanning the separation area with the accurate adsorption isotherm model and system properties. The influence of the column-to-column differences of any column property is more profound when the separation factor decreases. This could ultimately render isotopic separations by SMB extremely difficult.
7. The online monitoring of the SMB process is a valuable tool that improves the understanding of the process. It allows a continuous record of the concentration profiles inside the SMB unit, a constant comparison of experimental and calcu-

lated profiles, and online process control with a prompt response to changing separation conditions during this continuous process, when replacement columns are not available immediately. The process does not have to be interrupted to guarantee the separation constraints (albeit the production rate will decrease). In recent years, we have seen an increasing effort in the implementation of process control in the SMB process under linear conditions [47–49]. By using an online detection system, a better incorporation of process control can be done as well as its extension into nonlinear operating conditions.

8. The online detector combination described can be implemented in other preparative enantiomeric separations, such as closed-loop recycling and annular chromatography as well as in SMB application with solvent gradient and simulated moving bed reactors (SMBRs).
9. Finally, although emphasis was placed in this work on column-to-column fluctuations of the column porosity, the influence of any other parameter that controls the retention times or the migration velocity associated with any given concentration of the two solutes will be similar. For large columns, the batch-to-batch reproducibility of designer packing material (e.g., for enantiomeric separations) may become a critical issue [50].

6. Nomenclature

a	Henry isotherm coefficient
A	cm^2 – column cross section area
b	l/g or l^2/g^2 – adsorption isotherm parameters based on thermodynamics
C	g/cm^3 – liquid phase concentration
D_{ap}	cm^2/s – axial dispersion coefficient
F	Phase ratio
g	Amount of component 1 per volume and unit concentration
h	Amount of component 2 per volume and unit concentration
I.D.	cm – internal diameter of the column
k'	Retention factor
L_C	cm – column length
N	Theoretical number of plates
PR	$mg/s\ ml_{pack}$ – production rate of component 1 or 2
q	g/cm^3 – solid phase concentration
Q	cm^3/s – flow-rate
r	Dimensionless flow-rate
t	s – time
t^*	s – switching time
u	cm/s – liquid phase flow velocity
UV	mAU-response of the UV detector
z	Axial coordinate

Greek symbols

α	Separation factor
β	Margin parameter
ϵ	Overall void fraction

Subscripts

D	Desorbent
E	Extract
F	Feed
R	Raffinate
S	Solid
i	Feed component ($i=1, 2$)
j	Section (I, II, III, IV)
k	Number of columns
max	Maximal value of g (see above)
min	Minimal value of h (see above)
p	Pore or particle

Acknowledgements

This work was supported in part by grant CHE-00-70548 of the National Science Foundation and by the cooperative agreement between the University of Tennessee and the Oak Ridge National Laboratory. The authors are grateful to Chiral Technologies, Inc., for the generous gift of the ChiralPak AD columns and of small amounts of pure enantiomers of Tröger's base used for the acquisition of isotherm data, to PDR Chiral, Inc., for assistance in the polarimeter technology, to Prochrom for the generous gift of the SMB unit. They thank M.S. Smith, S. Khattabi, and D.E. Cherrak for their help.

References

[1] E. Küsters, G. Gerber, F.D. Antia, Chem. Eng. Sci. 40 (1995) 387.
[2] A. Seidal-Morgenstern, C. Blümel, H. Kniep, in: F. Meunier (Ed.), Fundamentals of Adsorption 6, Elsevier, Amsterdam, 1998, p. 303.
[3] M.P. Pedeferri, G. Zenoni, M. Mazzotti, M. Morbidelli, Chem. Eng. Sci. 54 (1999) 3735.
[4] D.C.S. Azevedo, L.S. Pais, A.E. Rodrigues, J. Chromatogr. A 865 (1999) 187.
[5] S. Khattabi, D.E. Cherrak, K. Mihlbachler, G. Guiochon, J. Chromtogr. A 893 (2000) 307.
[6] FDA, Chirality 4 (1992) 338.
[7] E.R. Francotte, in: Simulated Moving Bed: Basics and Applications, European Meeting, I.N.P.L., Nancy, L'Institut National Polytechnique de Lorraine, 1993, p. 35.
[8] D.B. Broughton, C.G. Gerhold, US Pat. 2 985 569 (1961).
[9] D.M. Ruthven, C.B. Ching, Chem. Eng. Sci. 44 (1989) 1011.
[10] H. Rhee, N.R. Amundson, Chem. Eng. Sci. 28 (1973) 55.
[11] G. Stori, M. Masi, S. Carra, M. Morbidelli, Chem. Eng. Sci. 44 (1989) 1329.
[12] G. Storti, M. Mazotti, M. Morbidelli, S. Carra, AIChE J. 39 (1993) 471.
[13] M. Mazotti, G. Storti, M. Morbidelli, J. Chromatogr. A 769 (1997) 3.
[14] T. Yun, Z. Bensetiti, G. Zhong, G. Guiochon, J. Chromatogr. A 758 (1997) 175.
[15] G. Zhong, G. Guiochon, Chem. Eng. Sci. 51 (1996) 935.
[16] B.J. Stanley, C.R. Foster, G. Giouchon, J. Chromatogr. A 761 (1996) 41.
[17] T. Yun, G. Zhong, G. Guiochon, AIChE J. 43 (1997) 935.
[18] G. Zenoni, M. Pedeferri, M. Mazzotti, M. Morbidelli, J. Chromatogr. A 888 (2000) 73.
[19] K. Mihlbachler, J. Fricke, T. Yun, A. Seidel-Morgenstern, H. Schmidt-Traub, G. Giouchon, J. Chromatogr. A 908 (2001) 49.
[20] A. Seidel-Morgenstern, G. Guiochon, J. Chromatogr. 631 (1993) 37.
[21] B. Toussaint, A.L.L. Duchateau, S. van der Wal, A. Albert, P. Hubert, J. Crommen, J. Chromatogr. Sci. 38 (2000) 450.
[22] L.S. Wigman, S. Douglas, S.S. Sekulic, J. Liq. Chromatogr. Rel. Technol. 23 (2000) 949.
[23] A.N. Diaz, F.G. Sandches, A.G. Pareja, J. Chromatogr. Sci. 36 (1998) 210.
[24] D.M. Goodall, Trends Anal. Chem. 12 (1993) 177.
[25] D. Bobbitt, D.W. Linder, G.W. Yanik, abstract of a paper presented at a meeting of the American Chemical Society, 2001.
[26] P. Marteau, N. Zanier-Szydlowski, A. Aoufi, G. Hotier, F. Cansell, Vib. Spectrosc. 9 (1995) 101.
[27] A. Epping, A. Jupke, H. Schmidt-Traub, M. Schulte, Chem. Eng. Sci., in press.
[28] A. Jupke, A. Epping and H. Schmidt-Traub, J. Chromatogr. A (2001) in press.
[29] C. Migliorini, M. Mazzotti, M. Morbidelli, AIChE J. 45 (1999) 1411.
[30] G. Guiochon, S.G. Shirazi, A.M. Katti, Fundamentals of Nonlinear and Preparative Chromatography, Academic Press, Boston, MA, 1994.
[31] R.-M. Nicoud, A. Seidel-Morgenstern, Isolat. Purif. 2 (1996) 165.
[32] T. Yun, G. Zhong, G. Guiochon, AIChE J. 43 (1997) 2970.
[33] T.L. Hill, An Introduction To Statistical Thermodynamics, Addison-Wesley, Reading, MA, 1960.
[34] B. Lin, Z. Ma, S. Golshan-Shirazi, G. Guiochon, J. Chromatogr. 475 (1989) 1.
[35] D.M. Ruthven, M. Goddard, Zeolites 9 (1986) 276.
[36] M. Diack, G. Guiochon, Anal. Chem. 63 (1991) 2608.
[37] K. Mihlbachler, M. DeJesus, M.J. Sepaniak, K. Kaczmarski, A, Seidel-Morgenstern, G. Guiochon, manuscript in preparation.
[38] K. Mihlbachter, Dissertation, in preparation.
[39] M. Sarker, G. Guiochon, J. Chromatogr. A 709 (1995) 227.
[40] www.chrialtechnologies.com, 12 December 2000.
[41] E. Glueckauf, J. Chem. Soc. (1947) 1302.
[42] F.G. Helferich, G. Klein, Multicomponent Chromatography, Marcel Dekker, New York, 1970.
[43] C. Blümel, P. Hugo, A. Seidel-Morgenstern, J. Chromatogr. A 827 (1998) 175.
[44] H. Kabir, G. Grevillot, D. Tondeur, Chem. Eng. Sci. 53 (1998) 1639.
[45] D.W. Marquardt, J. Soc. Appl. Math. 11 (1963) 431.
[46] G. Biressi, O. Ludemann-Hombourger, M. Mazzotti, R.-M. Nicoud, M. Morbidelli, J. Chromatogr. A 876 (2000) 3.
[47] E. Kloppenburg, E.D. Gilles, J. Process Control 9 (1999) 41.
[48] D.-J. Wu, Z. Ma, N.-H.L. Wang, J. Chromatogr. A 855 (1999) 71.
[49] K.-U. Klatt, F. Hanisch, G. Dünnebier, S. Engell, Comput. Chem. Eng. 24 (2000) 1119.
[50] M.S. Smith, G. Guiochon, J. Chromatogr. A 827 (1998) 241.